INDUSTRIAL DEMONSTRATION OF ARC DETECTION IN DC ARC FURNACES

C. J. Hockaday[1], Q. G. Reynolds[2], D. T. Jordan[3]

[1]Mintek, Private Bag X3015, Randburg, 2125, South Africa; chrish@mintek.co.za
[2] Mintek, Private Bag X3015, Randburg, 2125, South Africa; quinnr@mintek.co.za
[3] Mintek, Private Bag X3015, Randburg, 2125, South Africa; dominicj@mintek.co.za

ABSTRACT

The successful operation of DC plasma arc furnaces depends to a large extent on gaining a fundamental understanding of the arc phenomenon itself, and ensuring its presence in the furnace at all times. This is particularly important when operating in brush-arc mode, where the electrode tip is located in close proximity to the slag.

A method for confirming the presence of an arc in a DC circuit has been developed and successfully demonstrated on medium-scale pilot-plant facilities using characteristic frequency spectra on the anode-cathode voltage caused by the arc dynamics. The system has since been applied to a large-scale industrial furnace. Taking into account the order of magnitude differences in electrical and geometrical scale, the results are consistent with those obtained on pilot-scale tests, demonstrating that the arc-detection technology is applicable to production-scale furnaces.

1. INTRODUCTION

In a closed DC furnace, the arc is the primary heating and stirring element, by way of converting electrical energy to thermal energy and transferring it to the bath. The arc forms part of a series circuit, comprising the DC power supply, choke, bus bars and the slag bath. As a result, the majority of the operating voltage sourced from the power supply is divided between the arc and the bath.

The degree of split between the arc and bath is dependent on arc length and the combination of operating current and slag resistivity. The longer the required arc, the larger the voltage dropped across it. Similarly, the deeper and more resistive the slag, the higher the volt drop.

In designing a DC furnace, the power supply must be able to provide adequate voltage to the arc when taking into account anticipated slag resistivities and operating currents. Providing this "headroom" can add significant capital cost and it may therefore be more desirable to operate at reduced arc lengths. Brush-arc operation requires a lower total voltage, while retaining the process advantages of operating with an arc presence [1]. Operating at such short arc lengths may make it difficult to continuously maintain the electrode above the slag layer.

A further consequence of the dependence on slag resistivity is that if the properties of the actual slag produced vary significantly from the design parameters, even a well-designed power supply may not be able to sustain a suitable arc. Given the importance of the arc in these processes and the closed geometry of DC furnaces, under these circumstances it would be beneficial to be able to determine the existence of an arc at any given time.

A method to determine the presence of an arc has been devised and previously demonstrated on pilot-scale furnaces at Mintek [2][3]. The design has subsequently been optimised and applied to a full-size industrial furnace.

2. MODELLING

2.1 Theoretical treatment

The transient behaviour of the arc results from the interaction of the various field variables that describe the plasma system. These field variables are in turn described by the fundamental equations governing the physical phenomena relevant to magneto-hydrodynamic flow, and include fluid flow (the Navier-Stokes equations), heat transfer (the energy conservation equation) and electromagnetism (Maxwell's equations). More details are provided in [4].

A theoretical model was previously obtained by treating the arc as a purely inertial response system [3]. This results from a simplification of the Navier-Stokes equation governing the velocity field **v**, and hence the shape of the arc column over time is as follows:

$$\rho \frac{\partial \mathbf{v}}{\partial t} + (\rho \mathbf{v} \cdot \nabla)\mathbf{v} + \nabla P = \nabla \cdot (\mu \nabla \mathbf{v}) + \mathbf{j} \times \mathbf{B} \qquad (1)$$

Here, □ is the plasma density, *t* is time, *P* is pressure, □ is plasma viscosity, **j** is the local current density, and **B** is the local self-magnetic field that forms as a result of the current flow.

Over short time scales and in the region near to the arc's attachment to the graphite electrode where much of the dynamic behaviour originates, the Lorentz driving force term **j**×**B** tends to dominate (1). The arc's response may therefore be crudely approximated using:

$$\rho \frac{\partial \mathbf{v}}{\partial t} = \rho \frac{\partial^2 \mathbf{r}}{\partial t^2} \approx \mathbf{j} \times \mathbf{B} \quad (2)$$

Here, **r** is a displacement vector related to the position of the arc column in space. It is interesting to examine the dependence of the Lorentz term on furnace current. Inside the body of the arc, and particularly near the cathode spot on the graphite electrode, the current density tends to be approximately constant due to the limitations of thermionic emission from the graphite surface [5]. The cross-sectional area of the arc therefore increases in proportion to the furnace current, and the resulting peak magnetic field also scales proportionally – this can be thought of by analogy to the magnetic field generated around a long straight conductor, which scales proportionally to the current carried by the conductor. The Lorentz force term therefore scales approximately proportionally to furnace current, and may be described as:

$$\mathbf{j} \times \mathbf{B} = \mathbf{C_F} I \quad (3)$$

where $\mathbf{C_F}$ is a normalised vector function describing the time-dependence of noise and other disturbance signals coming from the power supply, grid, and environment, and *I* is the furnace current.

The Fourier transform of (2) is taken, following the same analysis presented in [3]. This gives:

$$-(2\pi\omega)^2 \mathcal{F}(\mathbf{r}) = \frac{\mathcal{F}(\mathbf{j} \times \mathbf{B})}{\rho} \quad (4)$$

Substituting (3) into (4), taking the magnitude of both sides, and taking the logarithm then produces:

$$\log_{10}|\mathcal{F}(\mathbf{r})| = \log_{10}\left[\frac{|\mathcal{F}(\mathbf{C_F} I)|}{4\pi^2 \rho}\right] - 2\log_{10}\omega \quad (5)$$

The furnace current may be brought out of the Fourier transform since it is a constant value and the transform is linear. Decomposing the first term on the right-hand side then gives:

$$\log_{10}|\mathcal{F}(\mathbf{r})| = \log_{10}\left[\frac{|\mathcal{F}(\mathbf{C_F})|}{4\pi^2 \rho}\right] + \log_{10} I - 2\log_{10}\omega \quad (6)$$

This relationship would be expected to hold across a range of furnace scales (as defined by the current *I*), with the first term on the right-hand side then capturing the scale and frequency independent effects. If a white-noise signal is assumed for $\mathbf{C_F}$, the relationship in (6) may be illustrated as shown in Figure 1.

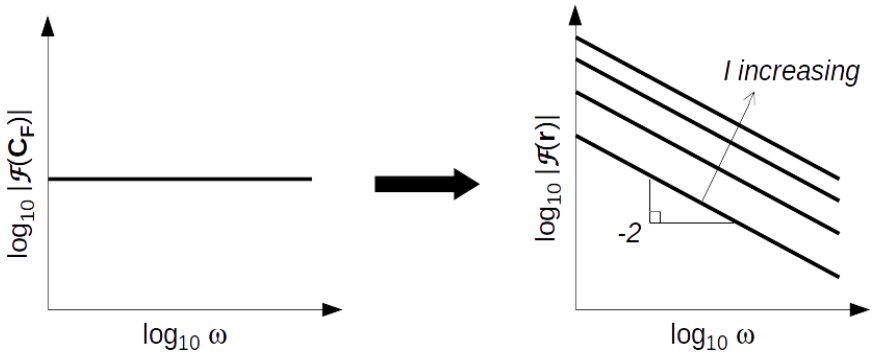

Figure 1: Dependence of Fourier transformed variables on frequency and furnace current

As **r** effectively determines the shape of the arc and therefore the voltage and other measurable parameters in this model, it would seem that arcs may be detected using voltage signals measured on DC furnace circuits by performing a Fourier transform operation on the data and seeking parts of the spectrum that exhibit a two decades per decade falloff. This falloff may also be expected to shift to higher frequency ranges as the furnace current increases.

2.2 Computational modelling results

The analysis method for arc detection was assessed using results generated by computational models of the DC plasma arc. These models use high-fidelity numerical solutions of the differential equations of magneto-hydrodynamics in order to track the evolution of the temperature, velocity and electromagnetic fields in and around the arc in space and time.

For this study two-dimensional, planar models of the arc region were used. These models are less mathematically rigorous than their three-dimensional counterparts, but have the advantage of being far less computationally demanding when used in parameter variation studies. Their ability to reproduce realistic arc behaviour has been demonstrated in previous publications [4]. The operating parameters used for the modelling work are shown in Table 1.

Table 1: Parameters used in computational arc model

Parameter	*Value*	*Parameter*	*Value*
Region dimensions	0.2 m x 0.05 m	Arc currents	200 A, 600 A, 1000A
Electrode diameter	0.05 m	Mesh resolution	1024 x 256
Cathode spot current density	3.5 x 10^7 A/m^2	Simulation time	10 ms
Plasma gas	Air	FFT sample time	5 ms – 10 ms

The models use a "flash start" initial condition, in which the arc is struck through a cloud of hot conductive plasma. Once the arc is established and the initial conditions decay, a sample of the time-dependent arc voltage is taken and subjected to Fourier analysis. A power-law equation is then fitted to the falloff section of the Fourier spectrum in accordance with equation (6).

The temperature fields from the end of the simulations are shown in Figure 2. There is noticeably more turbulence and high-velocity mixing as the arc current is increased.

(a) 200A (b) 1000A

Figure 2: Temperature fields from 2D arc models at 10ms
Scale: 2000 K (black) to 15000 K (blue/white)

The sampled voltage data is shown plotted against time in Figure 3. The increase in frequency of the chaotic motion of the arc is noticeable in the voltage traces. Completing the Fourier transform of the sampled data then gives the results shown in Figure 4, shown with fitted power-law curves. It can be seen that increasing the arc current in the model shifts the falloff section appreciably toward higher frequencies.

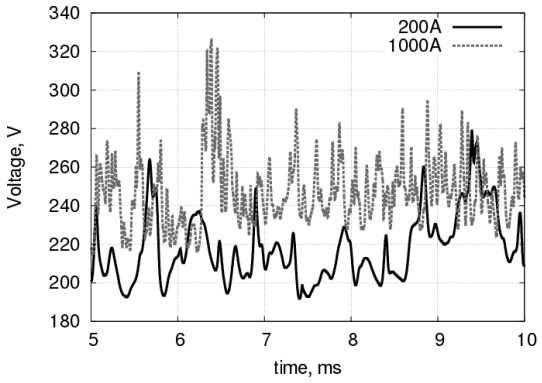

Figure 3: Model voltage vs time

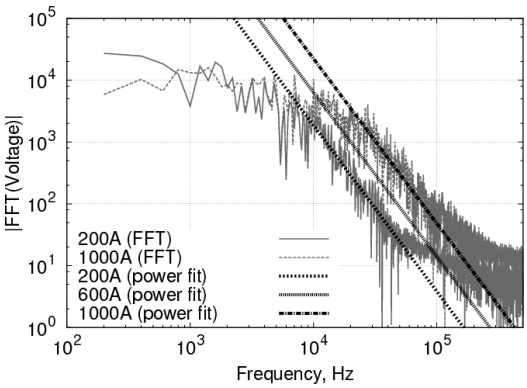

Figure 4: Spectral analysis of model voltage data

The fitted power law relationships are shown in Table 2. The gradient of the falloff remains largely constant across a substantial range of currents, but the intercept value increases, shifting the curves to the right of Figure 4.

Table 2: Fit parameters

Arc current	*Power-law fit (falloff region)*
200A	$\log_{10}\lvert\mathcal{F}(V)\rvert = 14.007 - 2.685\log_{10}\omega$
600A	$\log_{10}\lvert\mathcal{F}(V)\rvert = 14.427 - 2.656\log_{10}\omega$
1000A	$\log_{10}\lvert\mathcal{F}(V)\rvert = 15.005 - 2.664\log_{10}\omega$

From equation (6), the difference in the intercepts between 200 A and 600A would be expected to be $\log_{10}(600) - \log_{10}(200) = 0.477$, compared to the modelled value of 0.420. The difference in intercepts between 200 A and 1000A would be expected to be $\log_{10}(1000) - \log_{10}(200) = 0.699$, compared to the modelled value of 0.998.

Considering the degree of approximation required to arrive at both the theoretical and computational model results, this level of agreement may be considered acceptable. It is, however, expected that more extensive modelling and experimental work would be of use in validating the dependence of the falloff frequency on arc current.

3. MEASUREMENT EQUIPMENT

The prototype unit used to previously evaluate the theory on pilot-scale furnaces was modified and optimised to provide the required functionality with a minimal footprint. This facilitated transport to a remote furnace for evaluation.

The system comprises three main components. Firstly, the high (~1 kV – 2 kV) anode-cathode voltage is reduced to a measureable operating level and centred at earth potential for safety. The unit contains further over-voltage protection to prevent damage from extreme spikes which can occur in the event that the arc extinguishes causing an open circuit condition.

A high-speed data acquisition system captures data samples of the reduced voltage waveform, and a signal processing computer computes the spectral analysis to identify regions exhibiting the expected characteristics explained in the previous section.

Figure 5 below shows a block diagram of the components, as well as the connection points in the furnace circuit.

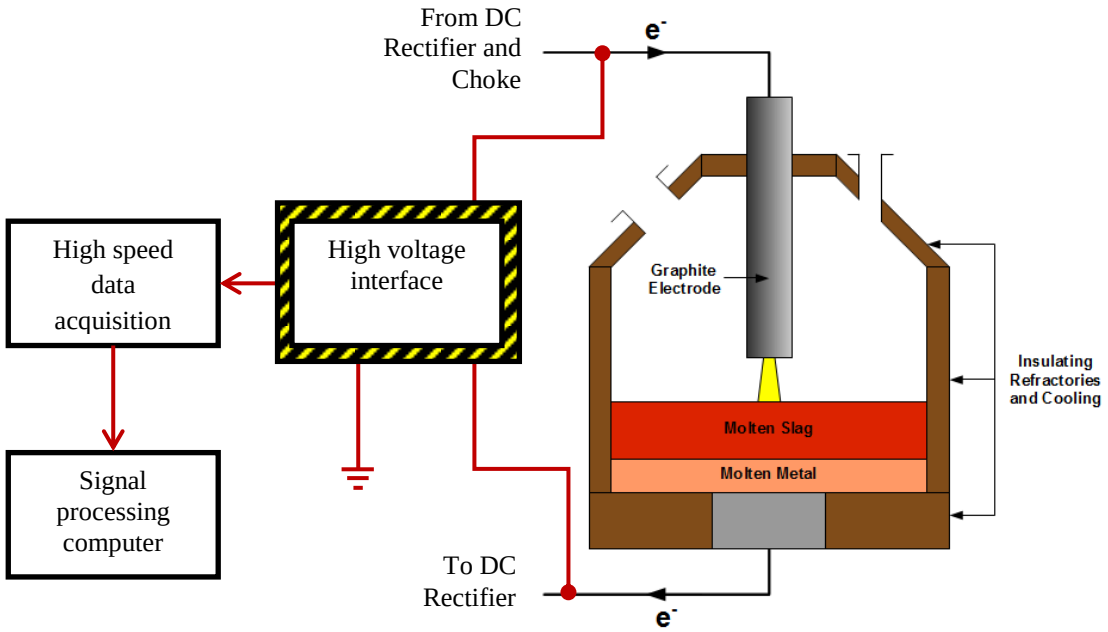

Figure 5: Block diagram of measurement system and connections to the furnace

3.1 Frequency Response of the Interface Unit

An additional consideration in designing for larger furnaces is the dependence of the roll-off frequency band on electrode current, as indicated in section 2 above. The system was therefore modified to operate with a much higher bandwidth than the initial prototype, which was limited to about 15 kHz.

Figure 6 below shows the bandwidth of the interface unit, together with the characteristic -2 dec/dec roll-off behaviour of arcs. The -3 dB point is at approximately 42 kHz. Since the response is that of a first-order low pass filter, the roll-off is significantly shallower than -2 dec/dec at frequencies below the order of 100 kHz.

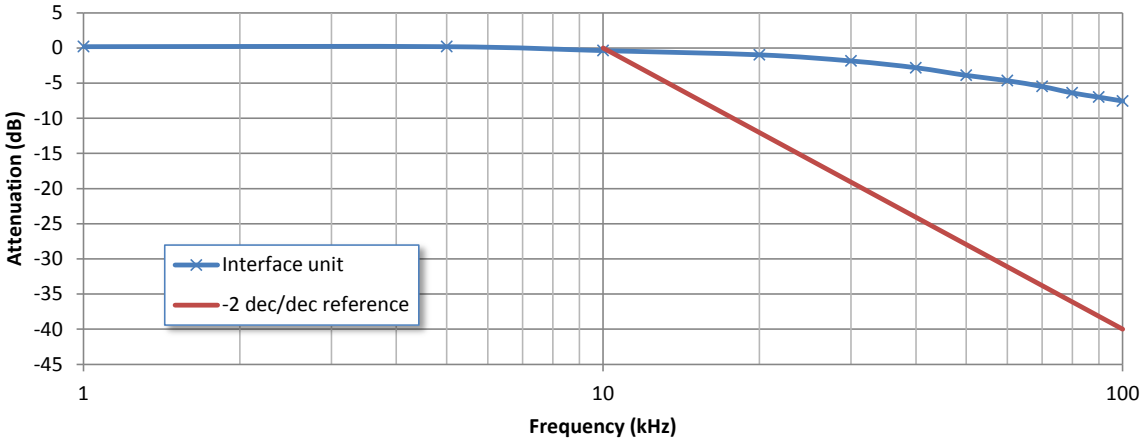

Figure 6: Frequency response of the high voltage interface unit

4. RESULTS AND DISCUSSION

A brief furnace shutdown was arranged to install the high-voltage interface unit on the 40 MW power supply. The unit was connected in parallel with the existing anode-cathode transducer. (The existing device had a limited bandwidth of the order of 5 kHz and was thus unsuitable for the high-frequency signal analysis required for this purpose.)

Upon furnace restart, a "touch-down" was performed to determine the electrode holder position with the electrode in close proximity to the slag. This provided a reference holder position that could be used to determine whether the electrode was subsequently operating in open arc or immersed conditions.

Figures 7 and 8 below represent high current (30 kA) operation with arc lengths greater than 30 cm.

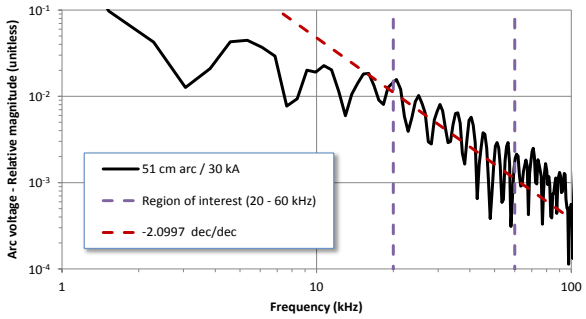

Figure 7: 51 cm arc / 30 kA
-2.10 dec/dec roll-off

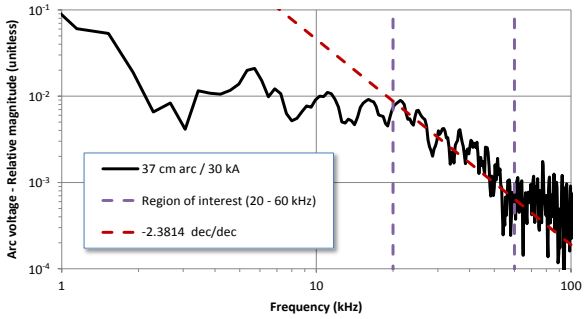

Figure 8: 37 cm arc / 30 kA
-2.38 dec/dec roll-off

It is clear that the characteristic -2 decade/decade roll-off is present on the industrial furnace. However, at higher currents, the frequency band where this occurs is significantly higher (20 kHz – 60 kHz) than previously experienced at low current (~1 kA) pilot-scale, where this behaviour was located in the 1 kHz – 5 kHz band [3].

Figures 9 and 10 illustrate the arc behaviour while immersed in the slag by about 30 cm, at a slightly lower current, since the furnace was idling.

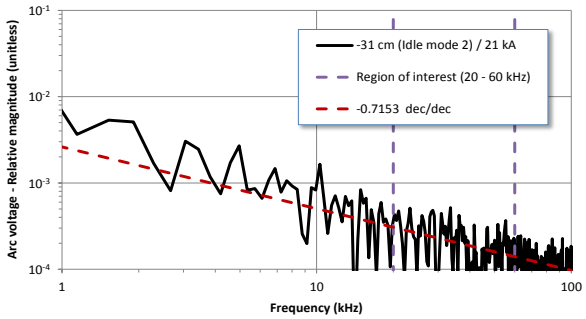

Figure 9: -31 cm (immersed) / 21 kA
-0.72 dec/dec roll-off

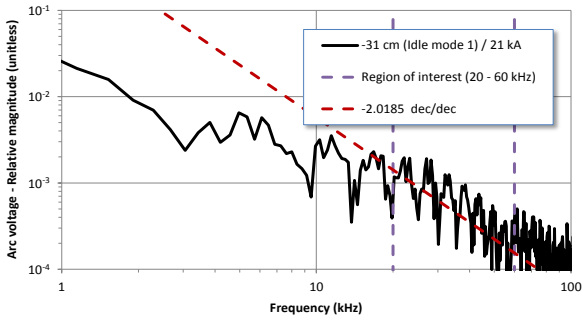

Figure 10: -31 cm (immersed) / 21 kA
-2.02 dec/dec roll-off

While immersed operation generally resulted in a much flatter frequency spectrum as expected (Figure 9), there were brief instances where behaviour typical of arcing occurred (Figure 10). This could be indicative of sporadic arcing, despite the electrode tip being immersed in the slag.

In the case of highly resistive slags, it is possible for arcing to continue even with the electrode submerged into the slag to a considerable degree. This is in accordance with the principle of minimum voltage, with an arc-slag system in series producing a lower overall voltage drop than simple conduction through the equivalent quantity of slag if the resistivity of the slag is sufficiently high.

If an arc is present with the electrode immersed into the slag layer, this would be expected to be a highly unstable condition with a large degree of fluid turbulence in and around the cavity formed around the arc beneath the slag surface (the “arc bubble”). This is predominantly due to the interaction between the very large thrust force generated by the arc jet at high currents [5] and the buoyancy forces acting on the surface of the arc bubble. This dynamic interaction is likely to lead to continuous, erratic expansion and collapse of the arc bubble, with the system momentarily reverting to purely resistive conduction before the arc re-establishes itself and the process repeats.

While unusual, this has been observed during pilot-scale testing of at least one other process at Mintek. Such behaviour could give rise to problems of superheated metal, if the arc remains present even when idling immersed at low power.

It is important to note that the voltage levels during the immersed tests were at the lower end of those that could be accurately measured by the arc monitor, and that quantisation noise during the digital sampling could thus have had an effect on the accuracy of those spectra. If this were the case however, it would seem more likely that the higher frequencies would be artificially exaggerated, thereby flattening the roll-off of the frequency spectrum, rather than accentuating it.

5. CONCLUSIONS

Refined modelling of plasma arc dynamics has shown that the previously explored principle of determining the existence of an arc through analysis of the Fourier spectrum is consistent across various operating scales, but exhibits a frequency dependence on the current.

Industrial testing of the arc detection principle confirms that the larger currents cause an upward shift in the frequency spectrum, but that the characteristic -2 decade/decade roll-off continues to apply.

Fixed installation of the instrument may be usefully applied as an operator-guidance tool on DC plasma arc furnaces, particularly where the presence of an arc is necessary, but otherwise difficult to verify.

6. ACKNOWLEDGEMENTS

This paper is published by permission of Mintek.

7. REFERENCES

[1] R.T. Jones, T.R. Curr. “Pyrometallurgy at Mintek”, Proceedings of Southern AfricanPyrometallurgy 2006 , ed. R.T. Jones (Johannesburg, South Africa: Southern African Institute ofMining and Metallurgy, 2006), Pp. 127-150.

[2] I.J. Barker, QG Reynolds, CJ Hockaday, DT Jordan (2013). “Measurement of Electrical Variables on a DC Furnace”, South African Provisional Patent Application No. 2013/083111

[3] Q.G. Reynolds, C.J. Hockaday, D.T. Jordan, and I.J. Barker (2014). “Arc Detection in DC Arc Furnaces”, Proceedings of the 143rd TMS Annual Meeting in: Celebrating the Megascale: An EPD Symposium on Pyrometallurgy in Honour of David GC Robertson, 16-20 February 2014, San Diego CA (USA), Pp. 157 – 167

[4] Q.G. Reynolds, R.T. Jones and B.D. Reddy (2010). "Mathematical and computational modelling of the dynamic behaviour of direct-current plasma arcs", Proceedings of the 12th International Ferroalloys Congress (INFACON XII), 6-9 June 2010, Helsinki (Finland), Pp. 789 - 801.

[5] B. Bowman (1994). "Properties of arcs in DC furnaces", Proceedings of the 52nd Electric Furnace Conference, 13-16 November 1994, Nashville TN (USA), Pp. 111 - 120.

[6] R.T. Jones. "DC Arc Furnaces – Past, Present and Future", Proceedings of the 143rd TMS Annual Meeting in: Celebrating the Megascale: An EPD Symposium on Pyrometallurgy in Honour of David GC Robertson, 16-20 February 2014, San Diego CA (USA), Pp. 135.